The HKU Scholars Hub   The University of Hong Kong   香港大學學術庫

Title	**Edge effect on thermally excited mag-noise in magnetic tunnel junction sensors**
Author(s)	**Zeng, T; Zhou, Y; Lin, KW; Lai, PT; Pong, PWT**
Citation	**The IEEE International Magnetics Conference (INTERMAG 2012), Vancouver, BC., 7-11 May 2012. In IEEE Transactions on Magnetics, 2012, v. 48 n. 11, p. 2831-2834**
Issued Date	**2012**
URL	**http://hdl.handle.net/10722/165288**
Rights	**IEEE Transactions on Magnetics. Copyright © IEEE.**

Edge Effect on Thermally Excited Mag-Noise in Magnetic Tunnel Junction Sensors

T. Zeng[1], Y. Zhou[2], K. W. Lin[3], P. T. Lai[1], and P. W. T. Pong[1]

[1]Department of Electrical and Electronic Engineering, The University of Hong Kong, Hong Kong
[2]Department of Physics, The University of Hong Kong, Hong Kong
[3]Department of Materials Science and Engineering, National Chung Hsing University, Taichung 402, Taiwan

Thermally excited magnetic noise (mag-noise) has gradually become a major concern in magnetic tunnel junction sensors. By conducting micromagnetic simulation, the spatial distribution of thermal mag-noise in the free layer (FL) was obtained under various hard bias (HB) field and applied field. It was demonstrated that the edges are the main contributor of thermal mag-noise in the FL. This result could be explained by the nonuniform distribution of the stiffness field around the edges. It was also found that both HB field and applied field could suppress the thermal mag-noise in edges. A relatively high applied field will decrease the influence of HB field on mag-noise in the edges.

Index Terms—Applied field, edges, free layer (FL), hard bias field, magnetic tunnel junction (MTJ), spatial distribution, thermal mag-noise.

I. INTRODUCTION

THERMALLY excited magnetic noise (mag-noise), originated from thermal magnetic fluctuations in magnetic tunnel junctions (MTJs), is of revived interests both theoretically and experimentally, due to its significant impact on the signal-to-noise ratio (SNR) of read/write heads in hard disk drives and magnetic sensors. As the recording density of hard disk drives reaches several Tbits/in^2 these years [1], the dimension of the storage cells is shrinking drastically, the thermally excited mag-noise has gradually become overwhelming when compared to Johnson and shot noise. In particular, the low frequency mag-noise (0–4 GHz) plays an extremely important role for the high speed operation of the read head. However, very few studies investigated how this thermal mag-noise is spatially distributed in MTJs, especially in the free layer (FL) of MTJs. In this paper, we investigate the spatial dependence of the thermal mag-noise in the FL utilizing micromagnetic simulation, which is conducive to the further understanding of the nature of mag-noise. The effect of spin transfer induced mag-noise is not extended here since the frequency range of the spin transfer induced mag-noise is much higher than our concerned frequency (0–4 GHz), which is beyond the scope of this paper.

II. MODELING AND COMPUTATION DETAILS

Fig. 1 shows the current-perpendicular-to-plane tunneling magnetoresistance (CPP-TMR) sensor structure used in our study, which is composed of FL (5)/spacer (0.9)/RL (2.5)/Ru (1)/PL (2.6)/AFM (thickness in nanometers), where RL, PL, and AFM stand for reference layer, pinned layer and antiferromagnetic layer, respectively (Ru layer and spacer layer are not shown in Fig. 1). The FL has saturation magnetization of $M_s = 860$ emu/cc and exchange stiffness
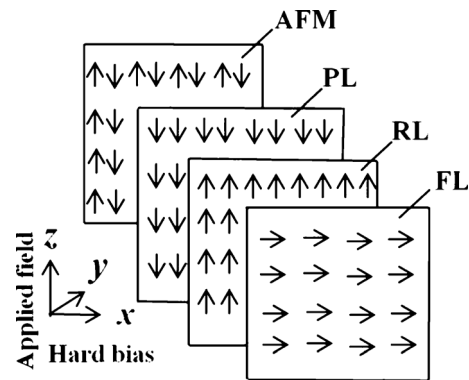
Fig. 1. Schematics of the MTJ sample structure (Ru layer and spacer layer are not included), and the directions of the hard bias field and applied field with the coordinate system.

$A_{ex} = 1.3 \times 10^{-6}$ erg/cm. The RL and PL have saturation magnetization $M_s = 1400$ emu/cc and exchange stiffness $A_{ex} = 2 \times 10^{-6}$ erg/cm [2]. The 1 nm Ru layer gives rise to an antiferromagnetic RKKY coupling of strength -1 erg/cm^2. Considering the PL is well-pinned, the effect of AFM is replaced by assuming a 2750 Oe field applied directly on PL. The hard bias (HB) field is provided by a uniform external field. The modeled MTJs have width $w = 100$ nm along the x-direction and heights h ranging from 60 to 140 nm.

The stochastic Landau-Lifshitz-Gilbert (LLG) equation is solved by utilizing object oriented micromagnetic framework (OOMMF) [3] with the thermal fluctuation term

$$\frac{d\overrightarrow{M}}{dt} = -|\gamma|\overrightarrow{M} \times \left(\overrightarrow{M}_{\text{eff}} + \overrightarrow{h}_{fl}(t)\right) - \frac{\alpha}{M_s}\left(\overrightarrow{M} \times \frac{d\overrightarrow{M}}{dt}\right) \tag{1}$$

where $\overrightarrow{h}_{fl}(t)$ is the thermal field modeling the Gaussian random process, with the variance of each cell written as

$$V_{ar} = \frac{\alpha}{1+\alpha^2}\frac{2k_B T}{\gamma\mu_0 M_s V} \tag{2}$$

where M_s is the saturation magnetization, V is the volume of each cell. Since the exchange length $l_{ex} = \sqrt{A/2\pi M_s^2}$
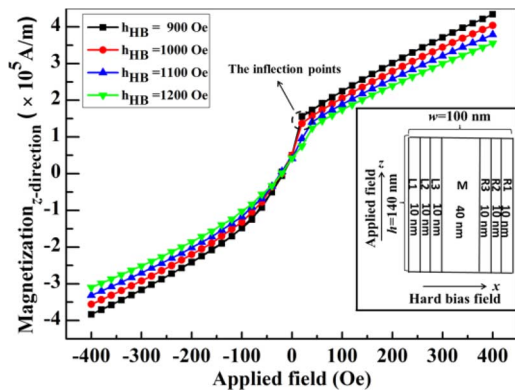
Fig. 2. Free-layer transfer curves for 100×140 nm dimension at various HB fields. Inset is the sample geometry and the orientation of the fields applied on the sample. The area is divided into seven rectangular regions denoted as L1, L2, L3, M, R3, R2, and R1 (from left to right), respectively. The L1 and R1 are the edges of the area.

Fig. 3. Simulated thermal mag-noise spectrum densities of different regions in free layer for 100 nm $\times 140$ nm dimension at 900 Oe HB field and zero applied field.

is around 7 nm, the mesh size is set as $5 \times 5 \times 2$ nm^3. The damping constant is $\alpha = 0.02$. The thermal fluctuations are simulated at $T = 60\ ^\circ$C which is below the Curie temperature. It is well justified for situation where the dynamics is adiabatic and close to equilibrium [4].

The magnetization configurations are obtained at each time step for sufficiently long time (10^{-7} sec) and collected every 10^{-11} sec. The noise power spectrum density (PSD) is calculated by the fast Fourier transform (FFT) from the time-varying magnetization.

III. SIMULATION RESULTS AND ANALYSIS

A. Free-Layer Transfer Curves

The free-layer transfer curve as a function of the applied field is depicted in Fig. 2 at various HB fields for a sample with a cross-section area of 100×140 nm. Since the transfer curve at zero applied field is our main concern, the applied field is not stretched to ranges where the free layer magnetization is fully saturated. The hysteresis is eliminated when the HB field reaches 900 Oe. The "S" shape of the transfer curves become asymmetric when the HB field reaches 900 and 1000 Oe. The inflection points which arise at +20 Oe applied field demonstrates that FL magnetization is inclined to the $-z$-direction. As the HB field further increases to 1100 and 1200 Oe, this asymmetry gradually disappears. This phenomenon is attributed to the influence of the stray field from the RL. The stray field induced by RL has a tendency to align the magnetization of FL along with the opposite magnetization direction of RL. As the HB field increases, the hard biasing effect overwhelms the influence of stray field from RL, which renders the symmetry of the transfer curves. Due to the shape anisotropy of the FL [5], the offset of transfer curves is also observed for the HB field from 900 to 1200 Oe. However, as the HB field increases, the offset amplitude decreases.

B. Noise Spectrum of Different Regions in the Free Layer

The HB field is kept at 900 Oe where the maximum sensitivity is obtained. As shown in the inset of Fig. 2, the FL is divided into seven rectangular regions denoted as L1, L2, L3, M, R3, R2, and R1 (from left to right), respectively. The dimensions of
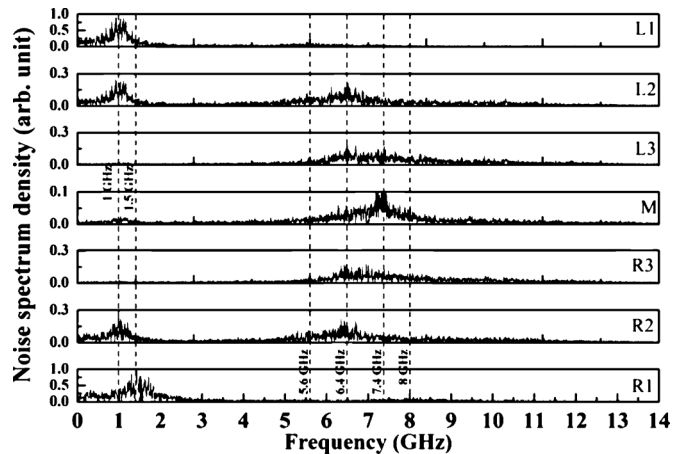
the regions are also illustrated. The L1 and R1 are the edges of the FL.

The normalized noise PSDs of the seven regions are calculated and shown in Fig. 3. It can be observed that in L1 and R1 regions, the 1 GHz low-frequency peak in L1 and 1.5 GHz low-frequency peak in R1 are dominant. The middle-frequency peaks located at 5.6 GHz in L1 and 8 GHz in R1 (the amplitudes are not obvious due to the relatively large scale of the vertical axis). As for the L2 and R2 regions, both of the low-frequency peaks are located at 1 GHz while their amplitudes are reduced to 20% of the peak amplitudes of L1 and R1. The 6.4 GHz middle-frequency peaks arise with comparable amplitudes to the low-frequency peaks in L2 and R2 regions. In L3 and R3 regions, the low-frequency peaks are fully suppressed and the 6.4 GHz middle-frequency peaks also get suppressed with the amplitudes decreased by 50% compared to the middle-frequency peaks in L2 and R2. The ranges of the middle-frequency peaks in L3 and R3 are much wider than in L2 and R2. For the M region, its middle-frequency at 7.4 GHz peak has been significantly suppressed while the low-frequency peak is fully suppressed.

The middle-frequency peaks can be ascribed to the ferromagnetic resonance (FMR). According to Smith [6], for magnetic thin-film element, the FMR peaks are well described by the zero-temperature, static stiffness fields model by the following equation:

$$\omega_0 = \frac{\gamma \sqrt{H_{xx} H_{yy}}}{\sqrt{1 + \alpha_{xx} \alpha_{yy}}} \tag{3}$$

$$H_{xx} = B_s(N_{xx} - N_{zz}) + H_k + H_z \tag{4}$$

$$H_{yy} = H_{xx} + B_s(N_{yy} - N_{xx}) \tag{5}$$

where γ is the gyromagnetic factor, $B_s = 4\pi M_s$, α_{xx}, and α_{yy} stand for the damping tensors of x-axis and y-axis components, respectively. It is assumed that the value $\alpha_{xx} \alpha_{yy}$ is far less than 1. H_k is the uniaxial anisotropy and H_z is the dc bias field oriented along the easy axis. Approximating the sample shape as an ellipsoid [7] where the sensor dimension ratios are height/length $= 0.0357$ and width/length $= 0.7143$, the demagnetization factors of $N_{xx} = 0.0316$, $N_{yy} = 0.93617$, and $N_{zz} = 0.03223$ are employed. The calculated FMR peak is

around 6.19 GHz, which agrees quite well with the simulation of 6.4 GHz.

However, the above description of the FMR is not applicable for L1, R1 and M regions. The reason why the thermally excited ferromagnetic resonance exhibits peaks at around 5.6 GHz in L1 and 8 GHz in R1 are mostly because a nonuniform distribution of the stiffness field H_{stiff} around the edges. H_{stiff} is determined by the competition among applied field, anisotropy, and HB field [8]

$$H_{\text{stiff}} = H_k \cos 2\phi + H_x \cos \phi + H_y \sin \phi \qquad (6)$$

where H_k is the anisotropy field, H_x and H_y are the total fields acting longitudinally and transversely, respectively. ϕ stands for the angle between the magnetization direction of FL and RL. A large demagnetization field around the edges will soften the edges and result in the reduction of stiffness field. On the other hand, the HB field can result in the increase of the anisotropy and harden the edges. The competition between the demagnetization field and the hard-bias field makes the stiffness field highly nonuniform between the edge regions and the central regions. Since the frequency of the FMR is scaled approximately with the square-root of the FL stiffness field [9], different frequencies of FMR peaks are obtained around the edges when comparing with other regions. For the more central regions, the influence of demagnetization would be gradually weakened and the H_{stiff} distribution could be more uniform. Thus we see the consistent FMR peaks in L2, L3, R2, and R3. For the central region M, the influence of demagnetization field could almost be neglected. We see an increase of the H_{stiff} and an increase of frequency of FMR peak to 7.4 GHz.

C. Low-Frequency Thermal Mag-Noise Spatial Distribution

The thermally excited low-frequency mag-noise PSDs in Fig. 3 could not be entirely interpreted by utilizing the model mentioned above. Here the mag-noise density is integrated from 0 to 4 GHz in each of these seven regions. The relation between the integrated low-frequency mag-noise and the spatial location under various HB field and zero applied field is depicted in Fig. 4(a). It is found that at 900 Oe HB field and zero applied field, the integrated low-frequency mag-noise is increased by 1731.45% from the middle (M) to the left edge (L1), and by 1409.40% from the middle (M) to the right edge (R1). Similar trends are also observed for the cases with HB fields of 1000, 1100, and 1200 Oe. On the other hand, as shown in Fig. 4(b) where the applied field is 400 Oe instead of zero, the integrated low-frequency mag-noise is increased only by 124.02% from the middle (M) to the left edge (L1) and only by 175.18% from the middle (M) to the right edge (R1). Similar trends are also observed for the cases with HB fields of 1000, 1100, and 1200 Oe. These increases are ten times smaller than those in Fig. 4(a).

From Fig. 4(a), it is concluded that there exists low-frequency mag-noise distribution gradient from the edges to the middle at various HB fields. However, with relatively high applied field, this gradient vanishes as demonstrated in Fig. 4(b). This characteristic is due to the multi-domain formation [10].

The simulated FL domain structures and their corresponding schematic domain structures under three different states are illustrated in Fig. 5. Fig. 5(a) shows the initial state of FL without
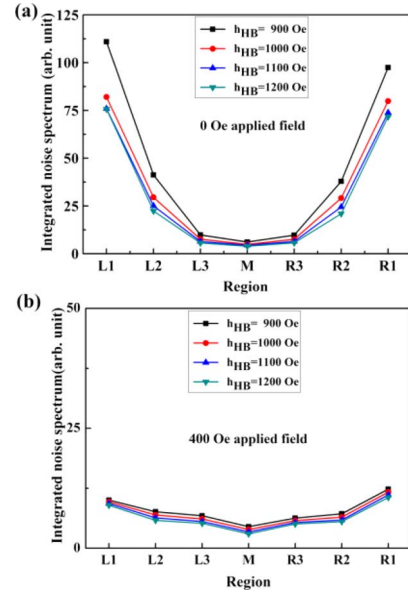

Fig. 4. (a) Integrated thermal mag-noise from 0 to 4 GHz versus different regions at various HB fields and zero applied field. (b) Integrated thermal mag-noise from 0 to 4 GHz versus different regions at various HB and 400 Oe applied fields.
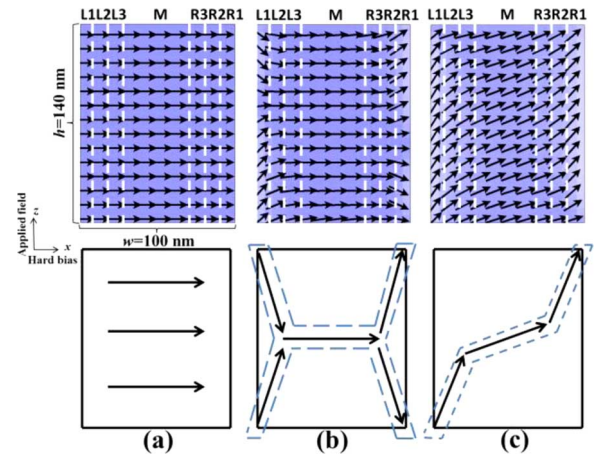

Fig. 5. (a) FL domain structure and its schematic structure at initial state. (b) FL domain structure and its schematic structure at 900 Oe HB field and zero applied field. (c) FL domain structure and its schematic structure at 900 Oe HB field and 400 Oe applied field.

any HB field or applied field. Fig. 5(b) shows the stable state under zero applied field and 900 Oe HB field. The stable state under 400 Oe applied field and 900 Oe HB field is shown in Fig. 5(c). It is observed that as the FL changes from the initial state [Fig. 5(a)] to the state under 900 Oe HB field [Fig. 5(b)], the domain structure transforms into two "C" shapes (one upwards and one downwards). The real-time domain stabilization process from the initial state [Fig. 5(a)] to the state under 900 Oe HB field [Fig. 5(b)] during simulation (not shown here) reveals that the magnetization of the edges exhibits prompt response while the magnetization in the middle responds reluctantly. Due to the nonuniform stiffness field, the edges are weakly pinned and spins here can be excited by the thermal field easily [5]. The magnetization around the edges thus behaves with larger tilting and oscillating amplitudes, which also result in an inconformity of magnetization directions among these seven regions.
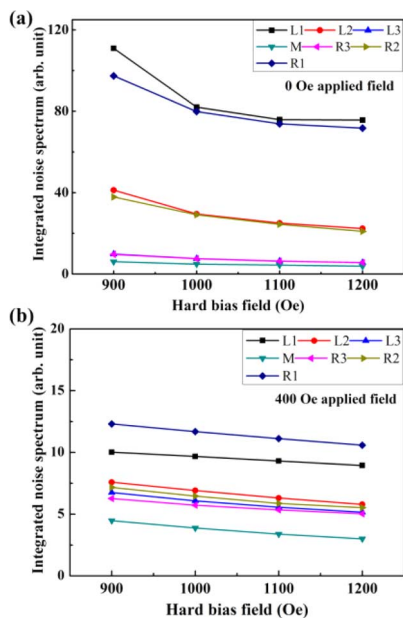
Fig. 6. (a) Integrated thermal mag-noise from 0 to 4 GHz versus various HB fields under different regions and zero applied field. (b) Integrated thermal mag-noise from 0 to 4 GHz versus various HB fields under different regions and 400 Oe applied field.

By observing the domain stabilization process from the state with zero applied field [Fig. 5(b)] to the state with 400 Oe applied field [Fig. 5(c)] during simulation in real-time (not shown here), it is found that the magnetization in the middle exhibits a more prompt motion than the magnetization in the edges. This results in the "S" shape domain structure in FL [Fig. 5(c)]. The quasi-uniform magnetization directions in these seven regions render a more stable demagnetization distribution in the edges. Thus the thermal excitation effect in the edges is gradually weakened by the applied field. As a result, the integrated low-frequency thermal mag-noise is suppressed. Therefore it is concluded the edge effect is the main contributor of the low-frequency thermal mag-noise in FL.

In order to further verify this conclusion, simulation and analysis were repeated with various sample sizes. The height h of the sample was varied from 60 to 120 nm while the width was kept at 100 nm. The same simulation results were obtained.

D. Hard Bias Field Effect

The relation between the HB field and the integrated low-frequency mag-noise in different regions under zero applied field and 400 Oe applied field can be observed from Fig. 6(a) and (b), respectively.

In Fig. 6(a), it can be seen that without applied field, when the HB field is relatively small (900 and 1000 Oe), its suppressing effect on the integrated low-frequency mag-noise is significant. This suppressing effect is particularly pronounced towards the edges (i.e., L1 and R1). This can be observed from the fact that as the HB field increases from 900 to 1000 Oe, the reduction of the mag-noise in L1 is 11.69 times larger than the reduction in L3, and the reduction in R1 is 15.39 times larger than the reduction in R3. After the HB field exceeds 1000 Oe, the mag-noise suppressing effect of the HB field is much weaker. Larger HB field only suppresses the mag-noise slightly in all the regions.

With 400 Oe applied, the mag-noise is relatively independent of the HB field as shown in Fig. 6(b). As the HB field increases from 900 to 1200 Oe, there is only a slight difference for the mag-noise in all the regions. The applied field could suppress the effect of HB field on edges.

IV. CONCLUSION

Edge effect on the thermal mag-noise spatial distribution was studied using micromagnetic simulation. It is shown that the edges are the main contributor of mag-noise in the FL. HB field can change the mag-noise spatial distribution in FL, especially suppress the mag-noise in the edges. However, the relative high applied field could restrain the effect of the HB field on the edges.

REFERENCES

[1] Y. Chen *et al.*, "2 Tbit/in² reader design outlook," *IEEE Trans. Magn.*, vol. 46, no. 3, pp. 697–701, Mar. 2010.

[2] N. Smith, J. A. Katine, J. R. Childress, and M. J. Carey, "Thermal and spin-torque noise in CPP (TMR and/or GMR) read sensors," *IEEE Trans. Magn.*, vol. 42, no. 2, pp. 114–119, Feb. 2006.

[3] M. J. Donahue and D. G. Porter, "OOMMF user's guide," (1.2a3 ver.) Oct. 30, 2000. [Online]. Available: http://math.nist.gov/oommf

[4] A. Rebei, L. Berger, R. Chantrell, and M. Covington, "1/f-type noise in a biased current perpendicular to the plane spin valve: A numerical study," *J. Appl. Phys.*, vol. 97, pp. 10E306–3, 2005.

[5] Y. Zhou, "Thermally excited low frequency magnetic noise in CPP structure MR heads," *IEEE Trans. Magn.*, vol. 43, no. 6, pp. 2187–2192, Jun. 2007.

[6] N. Smith, "Modeling of thermal magnetization fluctuations in thin-film magnetic devices," *J. Appl. Phys.*, vol. 90, pp. 5768–5773, 2001.

[7] J. A. Osborn, "Demagnetizing factors of the general ellipsoid," *Phys. Rev.*, vol. 67, pp. 351–357, 1945.

[8] G. C. Han *et al.*, "Hard bias effect on magnetic noise in different types of tunnel magnetoresistive heads," *IEEE Trans. Magn.*, vol. 44, no. 11, pp. 3597–3600, Nov. 2008.

[9] O. Heinonen and C. H. Seok, "Thermal magnetic noise in tunneling readers," *IEEE Trans. Magn.*, vol. 40, no. 4, pp. 2227–2232, Jul. 2004.

[10] C.-Y. You *et al.*, "Magnetic noise spectra and spin transfer torque of a magnetic tunnel junction with an exchange biased synthetic ferrimagnetic reference layer," *Curr. Appl. Phys.*, vol. 11, pp. e92–e94, 2011.